Structure, Vol. 13, 1435–1442, October, 2005, Published by Elsevier Ltd DOI 10.1016/j.str.2005.06.014

Intermediate States of Ribonuclease III in Complex with Double-Stranded RNA

Jianhua Gan, Joseph E. Tropea, Brian P. Austin, Donald L. Court, David S. Waugh, and Xinhua Ji[1,*]
Center for Cancer Research
National Cancer Institute
National Institutes of Health
Frederick, Maryland 21702

Summary

Bacterial ribonuclease III (RNase III) can affect RNA structure and gene expression in either of two ways: as a processing enzyme that cleaves double-stranded (ds) RNA, or as a binding protein that binds but does not cleave dsRNA. We previously proposed a model of the catalytic complex of RNase III with dsRNA based on three crystal structures, including the endonuclease domain of RNase III with and without bound metal ions and a dsRNA binding protein complexed with dsRNA. We also reported a noncatalytic assembly observed in the crystal structure of an RNase III mutant, which binds but does not cleave dsRNA, complexed with dsRNA. We hypothesize that the RNase III•dsRNA complex can exist in two functional forms, a catalytic complex and a noncatalytic assembly, and that in between the two forms there may be intermediate states. Here, we present four crystal structures of RNase III complexed with dsRNA, representing possible intermediates.

Introduction

Ribonuclease III (RNase III) belongs to a superfamily of double-stranded RNA (dsRNA) endoribonucleases (Court, 1993; Robertson et al., 1968) and has been found in most studied prokaryotes and eukaryotes (Court, 1993; Filippov et al., 2000; Krainer, 1997; Nicholson, 1996, 1999). It plays important roles in RNA processing, viral infection (Robertson et al., 1968), and posttranscriptional gene expression control (Court, 1993; Krainer, 1997; Wu et al., 2000). RNase III has gained added importance with the recent discoveries of the roles that its ortholog Dicer plays in RNA interference (RNAi), a broad class of gene silencing phenomena initiated by dsRNA in fungi, plants, insects, and animals (Bernstein et al., 2001; Carthew, 2001). The RNase III family can be divided into four subclasses with increasing molecular weight and complexity of the polypeptide, exemplified by RNase III, Rnt1p, Drosha, and Dicer, respectively (Blaszczyk et al., 2004).

Bacterial RNase III functions as a homodimer in which each polypeptide is composed of a single endonuclease domain (endoND) and a single dsRNA binding domain (dsRBD). It can affect RNA structure and gene expression in either of two ways: as a processing enzyme that cleaves dsRNA, or as a regulatory protein that binds but does not cleave dsRNA (Dasgupta et al., 1998; Oppenheim et al., 1993). As a dsRNA-processing enzyme, RNase III degrades both natural and synthetic dsRNA to small duplex products averaging 10–18 base pairs (bp) in length (Dunn, 1982; Robertson, 1982; Robertson and Dunn, 1975). As a dsRNA binding protein, RNase III binds certain substrates without processing but still influences gene expression by affecting RNA structures (Court, 1993; Dasgupta et al., 1998; Calin-Jageman and Nicholson, 2003; Oppenheim et al., 1993).

We have determined the endoND structures of *Aquifex aeolicus* RNase III (Aa-RNase III) with and without metal ions (Mn^{2+} or Mg^{2+}) bound in the active site (Aa-endoND, Aa-endoND•Mn^{2+}, and Aa-endoND•Mg^{2+}) and modeled a catalytic complex of full-length Aa-RNase III with dsRNA (Blaszczyk et al., 2001). The general location of the dsRNA in the catalytic complex was later supported by Zhang et al. (2004). We have also determined the crystal structure of an Aa-RNase III mutant that binds but does not cleave dsRNA (Dasgupta et al., 1998; Inada et al., 1989; Li and Nicholson, 1996) in complex with dsRNA (Aa-E110K•dsRNA), revealing the architecture of a noncatalytic assembly (Blaszczyk et al., 2004). Three major differences exist between the catalytic and noncatalytic forms of RNase III•dsRNA. First, the relative orientations of the endoND and dsRBD in the two forms are dramatically different (Figures 1A and 1B). Second, in the catalytic form, the two dsRBDs interact with the same dsRNA helix (Figure 1A). In the noncatalytic form, however, each dsRBD binds a different dsRNA helix (Figure 1B). Third, in the catalytic form the dsRNA substrate is bound in the catalytic valley (Figure 1A), whereas in the noncatalytic form the two dsRNA duplexes are completely out of the valley (Figure 1B). These variations are readily explained because the linker between the endoND and dsRBD is flexible. Figure 1C depicts the crystal structure of ligand-free RNase III from *Thermotoga maritima* (Tm-RNase III; Protein Data Bank code 1O0W), demonstrating that the seven-residue linker between the endoND and dsRBD ($_{145}$EGRVKKD$_{151}$ and $_{162}$KGEMLFD$_{168}$ in Aa- and Tm-RNase III, respectively) is flexible and allows the dsRBD to rotate and shift dramatically with respect to the endoND. Genetic studies have demonstrated that residues in the linker are essential for the dsRNA processing activity (Inada and Nakamura, 1995).

When RNase III is bound to dsRNA, we expect at least two stable conformations represented by our model of Aa-RNase III•dsRNA (Figure 1A) on the one hand and by the crystal structure of Aa-E110K•dsRNA (Figure 1B) on the other. These two modes of dsRNA binding would affect posttranscriptional gene expression by distinct mechanisms. As a dsRNA-processing enzyme, RNase III binds dsRNA in the valley (Figure 1A) where the active centers are located, allowing the substrate to be processed. As a dsRNA binding protein, RNase III binds dsRNA outside of the catalytic valley (Figure 1B) and therefore cannot process the bound dsRNA but still influences gene expression (Calin-Jage-

*Correspondence: jix@ncifcrf.gov
[1]Lab address: http://mcl1.ncifcrf.gov/ji.html

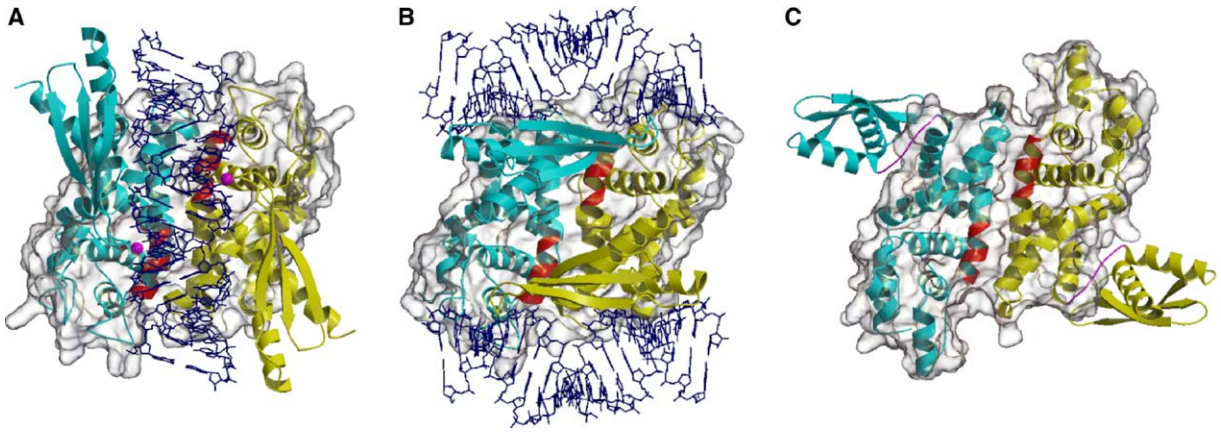

Figure 1. Three Previously Reported Conformations of RNase III

(A) A model of the catalytic form of Aa-RNase III•dsRNA (Blaszczyk et al., 2001) where the dsRNA is located in the catalytic valley of the enzyme.

(B) Crystal structure of the noncatalytic form of Aa-E110K•1-1 (Blaszczyk et al., 2004) showing that the dsRNAs are not bound in the catalytic valley.

(C) Ligand-free Tm-RNase III (PDB code 1O0W). The protein is illustrated as ribbon diagrams (helices as spirals, β strands as arrows, and loops as pipes) with the two subunits colored in cyan and yellow, respectively. The signature motif is highlighted in red and dsRNA is shown as blue sticks. For comparison, the three structures are oriented based on the alignment of their endoNDs, which are outlined with transparent surfaces. The figure was prepared with MOLSCRIPT (Kraulis, 1991), RASTER3D (Merritt and Bacon, 1997), and GRASP (Nicholls et al., 1991).

man and Nicholson, 2003; Court, 1993; Dasgupta et al., 1998; Oppenheim et al., 1993).

Our working hypothesis is that, in vivo, the RNase III dimer first binds a dsRNA with one of its two dsRBDs. If the dsRNA is of a sufficient length (at least two helical turns) and does not contain antideterminants (see below for details), an isomerization to the RNA-processing form may occur. This isomerization step, which was previously suggested using an active enzyme (Campbell et al., 2002), is essentially dependent on the flexible linker located between the endoND and the dsRBD (Blaszczyk et al., 2004), and is likely to be favored by an increase in binding affinity for the dsRNA due to its interaction with the other dsRBD and the catalytic valley of the endoNDs. In this study, we report four crystal structures of wild-type Aa-RNase III and two mutants (E110K and E110Q), each complexed with dsRNA. These structures appear to represent intermediate states of the RNase III•dsRNA complex leading to the two functional forms described above.

Results and Discussion

RNA 2, RNA 3, and RNA 4 Form Self-Complementary dsRNAs

Four different crystal structures of Aa-RNase III proteins in complex with dsRNA have been determined in this study. Two involve wild-type Aa-RNase III and the other two involve mutants Aa-E110K and Aa-E110Q. Mutations E110K and E110Q in Aa-RNase III correspond to E117K and E117Q in *Escherichia coli* RNase III (Ec-RNase III), respectively. These mutations abolish the endonucleolytic activity of Ec-RNase III without blocking its ability to recognize and bind dsRNA in vivo or in vitro (Court, 1993; Dasgupta et al., 1998; Inada et al., 1989; Li and Nicholson, 1996; Sun and Nicholson, 2001). We have shown that Aa-E110K forms a noncatalytic assembly (Figure 1B; Blaszczyk et al., 2004) with a self-complementary RNA 10-mer (GGCGCGCGCC; RNA 1) that forms 10 bp dsRNA helices (dsRNA 1-1) (Ryter and Schultz, 1998). In this study, an RNA 11-mer (RNA 2; see footnote of Table 1 for RNA sequences) that forms a 9 bp dsRNA with a two-nucleotide 3′ overhang on each end and a mismatch in the middle of the duplex (dsRNA 2-2) and two self-complementary RNA 12-mers (RNA 3 and RNA 4) that form 12 bp dsRNA helices (dsRNA 3-3 and 4-4, respectively) have been used. All of these dsRNA duplexes stack end to end as pseudocontinuous helices in the crystal lattices. In the four structures, each dimeric protein molecule binds two stacked dsRNA segments using only one of its dsRBDs (Figure 2). The final 2*Fo* – *Fc* electron density maps of dsRNA for the four structures are shown in Figure 2.

Aa-RNase III and Its E110K and E110Q Mutants Bind to One RNA Duplex

In the structure of the noncatalytic assembly (PDB code 1RC7; Blaszczyk et al., 2004), each of the two dsRBDs in the dimer binds independently to separate dsRNA helices (Figure 1B). In the catalytic model complexes (Blaszczyk et al., 2001; Zhang et al., 2004), however, a dimeric RNase III molecule binds one dsRNA helix with both dsRBDs (Figure 1A). It is most likely that the wild-type RNase III dimer in the cell first binds a dsRNA segment through one of its two dsRBDs. Under different circumstances, the conformational changes of the complex may lead to the formation of either a catalytic (Figure 1A) or a noncatalytic (Figure 1B) complex (Blaszczyk et al., 2004). Our structures of Aa-E110Q•2-2 (Figure 2A), Aa-RNase III•3-3 (Figure 2B), Aa-RNase III•4-4 (Figure 2C), and Aa-E110K•4-4 (Figure 2D) show that a dimeric RNase III can bind one dsRNA helix. In three out of the four complexes, the dsRNA is not

Table 1. Crystal Data, X-Ray Data, Structure Solution, and Refinement Statistics

	Aa-E110Q•2-2[a]	Aa-RNase III•3-3[b]	Aa-RNase III•4-4[c]	Aa-E110K•4-4[c]
Crystal				
Shape	plate	block	plate	plate
Dimensions (mm)	0.25, 0.20, 0.05	0.20, 0.30, 0.30	0.05, 0.20, 0.40	0.05, 0.15, 0.30
X-Ray Data				
Space group	$P2_1$	$P2_12_12_1$	$P2_12_12_1$	$P2_12_12_1$
Unit cell dimensions: a (Å)	60.59	86.43	85.27	84.49
b (Å)	118.36	95.91	61.95	61.63
c (Å)	61.90	166.00	131.75	131.11
β (°)	99.45	90.00	90.00	90.00
Resolution (Å)	30.0–2.10	30.0–2.80	30.0–2.50	30.0–2.90
Measured reflections	189,903	162,494	105,914	79,003
Unique reflections	42,826	31,417	21,859	14,293
Completeness (%), overall/last shell[d]	86.8/50.1	90.5/44.8	88.0/43.7	91.8/53.7
R_{merge},[e] overall/last shell[d]	0.084/0.365	0.084/0.361	0.148/0.367	0.060/0.270
$I/\sigma(I)$, overall/last shell[d]	14.5/2.56	12.6/1.2	9.1/1.1	22.4/1.7
Structure solution	Mol replacement	Mol replacement	Mol replacement	Difference Fourier
Start/search model	PDB code 1I4S	PDB code 1I4S	PDB code 1I4S	Aa-RNase III•3-3
Correlation coefficient	0.66	0.68	0.55	N/A
R factor	0.49	0.49	0.48	N/A
Refinement Statistics				
No. data in refinement	40,681	29,599	20,579	13,446
No. data for R_{free}	2,145	1,818	1,280	847
No. residues/protein atoms	438/3,659	875/7,314	442/3,694	439/3,668
No. nucleic acid atoms	920	1,992	1,012	1,012
No. heterogen atoms	35 (SO_4)	0	8 (Tris)	8 (Tris)
No. solvent atoms	387	94	188	36
Final R factor	0.208	0.243	0.226	0.223
Final R_{free}	0.238	0.314	0.296	0.292
Rmsd: bond lengths (Å)	0.006	0.005	0.006	0.004
Bond angles (°)	1.1	1.0	1.0	0.9
Estimated coordinate error (Å)	0.32	0.42	0.37	0.39
Overall B factor ($Å^2$)	52.7	62.5	62.8	70.7
Wilson B factor ($Å^2$)	47.5	49.9	56.6	61.9
Ramachandran statistics (%)				
Most favored ϕ/ψ values	95.1	84.8	89.8	84.0
Disallowed ϕ/ψ values	0.0	0.5	0.5	0.2

[a] 2-2: dsRNA formed by self-complementary sequence 5′-CGAACUUCGCG-3′.
[b] 3-3: dsRNA formed by self-complementary sequence 5′-AAAUAUAUAUUU-3′.
[c] 4-4: dsRNA formed by self-complementary sequence 5′-CGCGAAUUCGCG-3′.
[d] Last shell of X-ray diffraction data for Aa-E110Q•2-2, Aa-RNase III•3-3, Aa-RNase III•4-4, and Aa-E110K•4-4 is 2.18–2.10 Å, 2.90–2.80 Å, 2.59–2.50 Å, and 3.00—2.90 Å, respectively.
[e] $R_{merge} = \Sigma|(I - \langle I \rangle)|/\sigma(I)$, where I is the observed intensity.

bound in the vicinity of the catalytic valley (Figures 2A, 2C, and 2D), similar to that observed in the noncatalytic Aa-E110K•1-1 complex structure (Figure 1B). In the Aa-RNase III•3-3 complex, however, the dsRNA is found near the catalytic valley (Figure 2B) although the dsRNA is not in the valley as suggested for the catalytic binding (Figure 1A). Therefore, the four complex structures may represent possible intermediate states leading to the two functional forms of the RNase III•dsRNA complex.

The Relative Positioning of dsRNA and dsRBD Is Protein Dependent

Interactions between dsRBD and dsRNA are RNA sequence independent (Krovat and Jantsch, 1996; Manche et al., 1992; Polson and Bass, 1994; Ryter and Schultz, 1998). However, the relative positioning of the dsRBD and dsRNA is protein dependent. Previously, we reported that a difference existed in the arrangement of dsRNA 1-1 with respect to the dsRBD from Aa-RNase III (Aa-dsRBD) and that from the *Xenopus laevis* dsRNA binding protein A (Xl-dsRBD). In the two structures, dsRNA 1-1 rotated differently along its long axis by almost one bp while retaining its interactions with the dsRBDs (Blaszczyk et al., 2004). In this study, we observe a conserved dsRBD-dsRNA arrangement of Aa-RNase III in five complexes involving different dsRNAs: 1-1, 2-2, 3-3, and 4-4 (not shown). The RNA-independent nature of the dsRBD-dsRNA interaction made it possible to build a preliminary model of the catalytic complex (Blaszczyk et al., 2001), whereas the protein-dependent property of the dsRBD-dsRNA interactions renders it impossible to uniquely position the dsRNA with respect to the protein using the dsRBD•dsRNA structure of a non-RNase III protein.

A Symmetric dsRBD•dsRNA•dsRBD Structure

We have observed a symmetric dsRBD•dsRNA•dsRBD structure in the crystal of Aa-E110Q•2-2 in which the dsRNA 2-2 helix interacts with a second dsRBD from a symmetry-related complex (Figure 3A). Although dsRNA 3-3 and 4-4 also interact with symmetry-related dsRBDs,

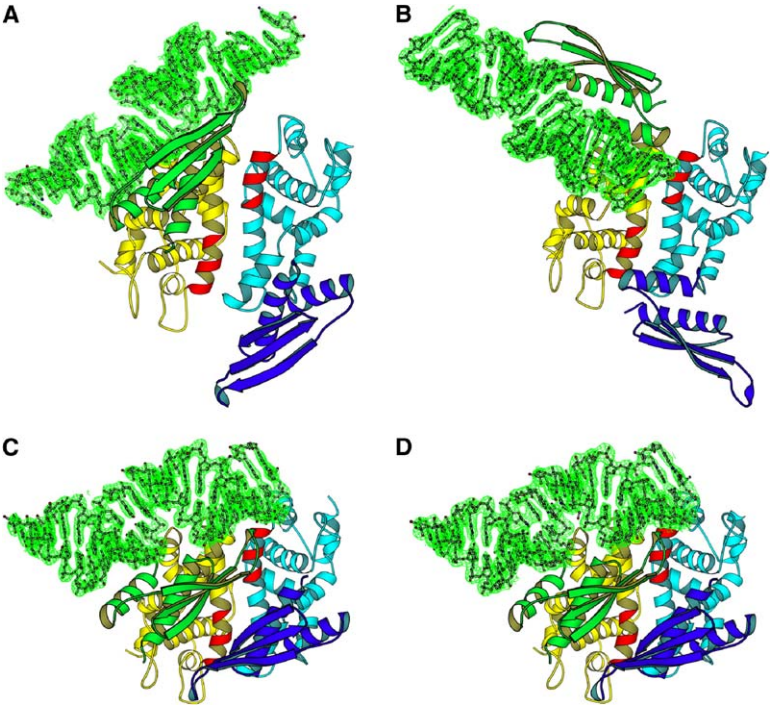

Figure 2. Four Crystal Structures of RNase III in Complex with dsRNA

(A) Aa-E110Q•2-2.
(B) Aa-RNase III•3-3.
(C) Aa-RNase III•4-4.
(D) Aa-E110K•4-4.

A biological dimer is shown for each structure. The endoND and dsRBD of one subunit are colored yellow and green, respectively, while the endoND and dsRBD of the other subunit are colored cyan and blue, respectively. The RNase III signature motif is highlighted in red. Helices, β strands, and loops are drawn as spirals, arrows, and pipes, respectively. The dsRNA are illustrated as stick models outlined by corresponding electron density (green net, final $2F_o - F_c$ contoured at 1 σ). The figure was prepared with BOBSCRIPT (Esnouf, 1997).

the two dsRBD-dsRNA interfaces are not identical in Aa-RNase III•3-3 (Figure 3B) and the arrangement of the two dsRBDs is not symmetric in Aa-RNase III•4-4 and Aa-E110K•4-4 (Figures 3C and 3D).

An important difference is observed between the pseudoduplex formed by dsRNA 2-2 and those of the other dsRNAs: the former adopts a regular A form helix (Figure 3A), whereas the others exhibit a kink between the stacking RNA duplexes (Figures 3B–3D), including also the pseudoduplex formed by dsRNA 1-1 (Blaszczyk et al., 2004). The structural basis for this difference could be the two-nucleotide 3′ overhang at each end of dsRNA 2-2, which may facilitate the formation of an A form duplex. Duplexes 1-1, 3-3, and 4-4 do not have the two-nucleotide 3′ overhang, and may result in the irregularity at the stacking points. Therefore, a regular A form duplex is perhaps necessary for the dsRNA to interact with two dsRBDs in a symmetric manner.

The Flexible Linker Is Essential for the Function of RNase III

As shown in Figure 1, the conformational change of RNase III depends upon a seven-residue linker ($_{145}$EGRVKKD$_{151}$ and $_{149}$PGDKQKD$_{155}$ in Aa- and Ec-RNase III, respectively) between the endoND and dsRBD. It has been shown that the Q153P substitution in Ec-RNase III abolishes its RNA cleavage activity without affecting its ability to bind dsRNA (Inada and Nakamura, 1995). Although this residue is not conserved among bacterial RNase III proteins, the introduction of a Pro residue in the middle of the linker probably reduces its flexibility, which is probably essential for RNA processing activity. We suggest that the structural differences (Figure 2) observed in this study can also be ascribed to the flexibility of the linker. To date, we have determined five crystal structures of full-length Aa-RNase III proteins in complex with dsRNA, including Aa-E110K•1-1 (Figure 1B; Blaszczyk et al., 2004), Aa-E110Q•2-2 (Figure 2A, this work), Aa-RNase III•3-3 (Figure 2B, this work), Aa-RNase III•4-4 (Figure 2C, this work), and Aa-E110K•4-4 (Figure 2D, this work). In all five structures, the flexible linker is well defined, suggesting that the conformations observed in the crystal lattice are relatively stable, a characteristic feature of intermediates.

We also expect that the end-to-end stacking of the 10-mer (dsRNA 1-1), 11-mer (dsRNA 2-2), and 12-mer (dsRNA 3-3 and 4-4) dsRNA elements affects the stability of the entire structure. Because the concentration of these RNA elements is initially quite high under crystallization conditions, one might expect the independent binding of a dsRBD to two stacked RNA elements to occur, mimicking an RNA duplex with a total length ranging from 20 to 24 bp (Figure 2). Upon crystallization, the dsRNA elements are likely to stack in their most stable conformation that optimizes their interactions with the protein. For this to happen, the linker is likely to provide the flexibility of needed movement.

Hypothetical Pathways toward the Two Functional Forms of RNase III•dsRNA

Bacterial RNase III affects posttranscriptional gene expression by two different mechanisms through two distinct forms of the protein-dsRNA complex. The four RNase III•dsRNA structures reported here (Figure 2) may represent intermediate states leading to these two functional forms.

Figure 4 depicts hypothetical pathways leading to these two functional forms of RNase III•dsRNA, involving six conformations of the protein and protein-dsRNA

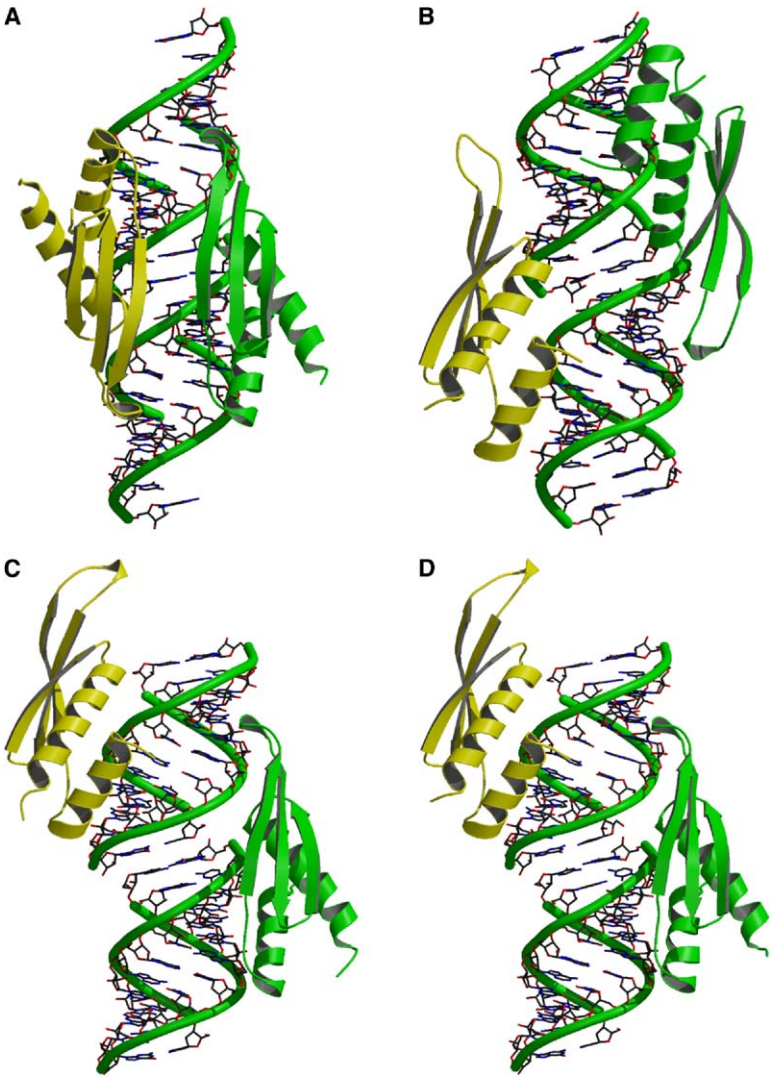

Figure 3. The Interaction between dsRNA and Two dsRBDs in Crystal Lattice

(A) Aa-E110Q•2-2.
(B) Aa-RNase III•3-3.
(C) Aa-RNase III•4-4.
(D) Aa-E110K•4-4.

The dsRBD•dsRNA complex (in green) and a symmetry-related dsRBD (in yellow) are shown for each structure. Helices, β strands, and loops are drawn as spirals, arrows, and pipes, respectively. The dsRNA are illustrated as backbone worms with stick models for nucleotides in the atomic color scheme (carbon in black, nitrogen in blue, and oxygen in red). The figure was prepared with MOLSCRIPT (Kraulis, 1991) and RASTER3D (Merritt and Bacon, 1997).

complex. The conformation of ligand-free RNase III (conformation A) is represented by a known crystal structure (PDB code 1O0W; Figure 4A). The four structures reported here reveal three distinct conformations of the protein-dsRNA complex (conformations B, C, and E) represented by Aa-E110Q•2-2 (Figure 4B), Aa-RNase III•3-3 (Figure 4C), and Aa-RNase III•4-4 (Figure 4E), respectively. The conformation of the catalytic (conformation D) form is represented by our model of the catalytic complex (Blaszczyk et al., 2001), whereas that of the noncatalytic (conformation F) form is represented by a known structure (Figure 4F; Blaszczyk et al., 2004).

In vivo, the ligand-free RNase III dimer (conformation A; Figure 4A) first binds one dsRNA with one of its two dsRBDs. The resulting complex may exhibit at least two possible conformations, B (Figure 4B) and E (Figure 4E), both with the dsRNA located completely out of the catalytic valley. Conformations B and E may be interchangeable via a "breathing-like" open-and-close movement of the enzyme, as indicated by the distance between the two dsRBDs. In conformation E (Figure 4E), the two dsRBDs pack against each other, whereas in conformation B (Figure 4B), the two dsRBDs are apart from each other. Therefore, the dsRBD•dsRNA complex in conformation B may readily rotate around the flexible linker in the counterclockwise direction, resulting in conformation C (Figure 4C). We expect that conformations B (Figure 4B) and C (Figure 4C) are interchangeable as well, although further rotation of the dsRBD•dsRNA moiety in conformation C (Figure 4C) leads to the catalytic conformation D. In contrast, the free rotation of dsRBD•dsRNA in conformation E (Figure 4E) may be hindered by the closely packed dsRBDs, resulting in the noncatalytic conformation F (Figure 4F). This can happen if the dsRNA is of an insufficient length (less than two helical turns), or an antideterminant exists either in the dsRNA, such as the special bulge-helix-bulge motif in dsRNA R1.1[CL3B] (Calin-Jageman and Nicholson, 2003), or in the protein, such as the E110K mutation in Aa-RNase III (Blaszczyk et al., 2004). Two individual mutations in Ec-RNase III (G44D and D155E) have also been reported, which abolish the dsRNA cleavage activity of RNase III via blocking the

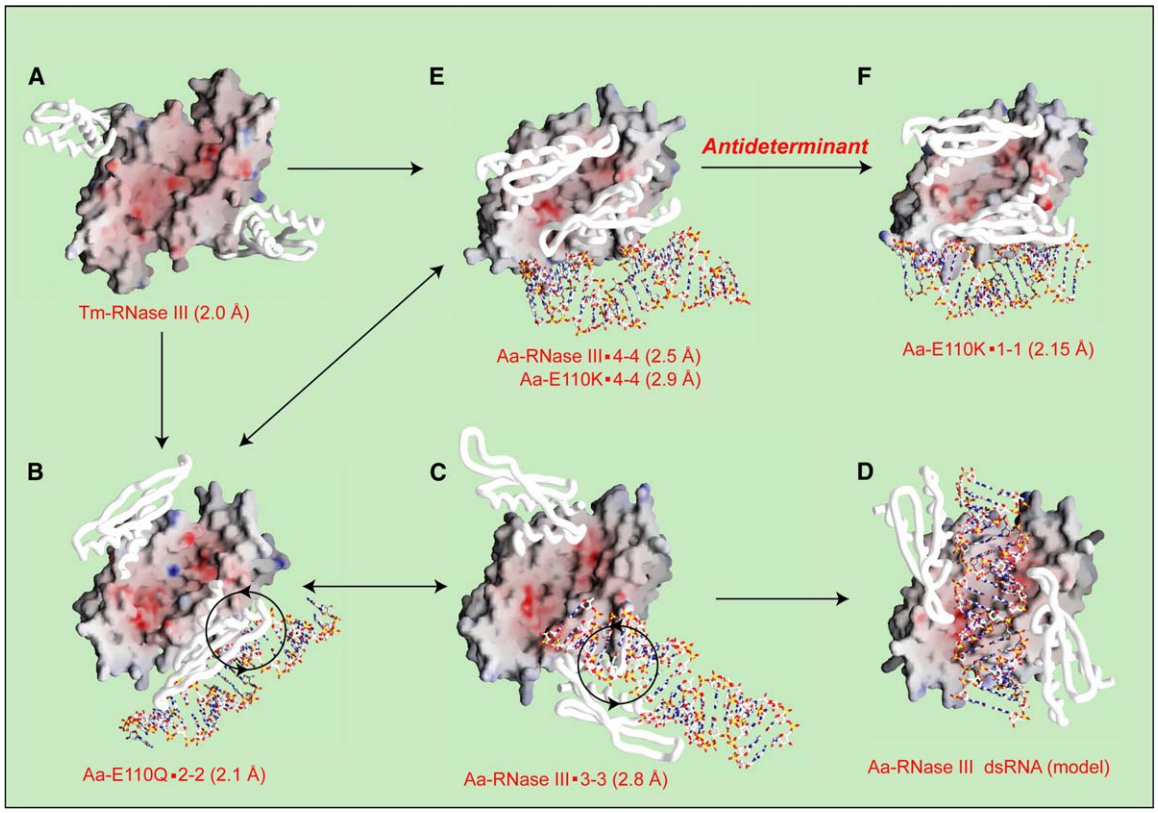

Figure 4. Hypothetic Pathways Leading to Two Functional Forms of the RNase III•dsRNA Complex

Six distinct states, conformations A–F, in the pathways are represented by (A) ligand-free Tm-RNase III (PDB code 1O0w), (B) Aa-E110Q•2-2 (this work), (C) Aa-RNase III•3-3 (this work), (D) RNA-processing form of Aa-RNase III•dsRNA (this work), (E) Aa-RNase III•4-4 and Aa-E110K•4-4 (this work), and (F) noncatalytic form of Aa-E110K•1-1 (Blaszczyk et al., 2004). The endoND is illustrated as a molecular surface with positive and negative potentials indicated by blue and red colors, respectively; the dsRBD is shown as a Cα backbone worm in white; and the dsRNA is represented as stick models in the atomic color scheme (carbon in white, nitrogen in blue, oxygen in red, and phosphorus in yellow). The circles indicate a possible rotation of the dsRBD•dsRNA moiety enabled by the flexible linker between the endoND and dsRBD; the direction of predicted rotation is indicated by arrowheads on the circles. The figure was created with GRASP (Nicholls et al., 1991). The orientation of the endoND moiety was kept constant.

initial recognition of the substrate (Bardwell et al., 1989; Inada and Nakamura, 1995), but not due to the formation of a noncatalytic assembly as described above.

Experimental Procedures

Construction of the Aa-E110Q Expression Vector

The plasmid expression vector that was used to produce the Aa-E110Q mutant was constructed by overlap extension PCR (Ho et al., 1989) and Gateway recombinational cloning. pHPK1409 (Blaszczyk et al., 2004) was used as the template for PCR. The PCR product was recombined into the entry vector pDONR201 (Invitrogen, Carlsbad, CA) and verified by sequence analysis. The open reading frame (ORF) encoding the E110Q mutant was then recombined into pET-DEST42 (Invitrogen), a derivative of pET11 (Novagen, Madison, WI), to create the expression vector pBA1492.

Protein Expression and Purification

The Aa-E110K protein was overproduced in *E. coli* and purified as described (Blaszczyk et al., 2004). The Aa-E110Q mutant was overproduced in *E. coli* BL21(DE3) CodonPlus-RIL cells (Stratagene, La Jolla, CA). Single antibiotic-resistant colonies were used to inoculate 100 ml of Luria-Bertani (LB) (Miller, 1972) supplemented with 100 μg/ml ampicillin and 30 μg/ml chloramphenicol. These cultures were grown with shaking (225 rev./min) to saturation overnight at 37°C and then diluted 33-fold into six 1 L preparations of fresh media resulting in an initial optical density of approximately $OD_{600\ nm}$ = 0.15. When the cells reached early log phase ($OD_{600\ nm}$ ~0.5), the temperature was reduced to 30°C and isopropyl β-D-thiogalactopyranoside (IPTG) was added to a final concentration of 1 mM. The cultures were incubated for 4 hr and pelleted by centrifugation at 5000 × g for 10 min at 4°C. The cell pellet was stored at −80°C.

Unless otherwise stated, all procedures were performed at 4°C. *E. coli* cell paste was suspended in ice-cold 50 mM sodium phosphate (pH 8.0), 25 mM NaCl buffer (buffer A) containing 1 mM benzamidine and Complete EDTA-free protease inhibitor cocktail tablets (Roche, Indianapolis, IN), and disrupted with an APV Gaulin model G1000 homogenizer (APV USA, Lake Mills, WI) at 10,000 psi. The homogenate was centrifuged at 30,000 × g for 30 min, and the supernatant was heat treated at 80°C for 20 min. After pelleting the insoluble material by centrifugation, the supernatant was filtered through a 0.22 μm polyethersulfone membrane and applied to a HiPrep 16/10 SP FF column (Amersham Biosciences, Piscataway, NJ) equilibrated with buffer A. The column was washed with ten column volumes of buffer A and eluted with a linear gradient of NaCl from 25 mM to 1 M. Fractions containing recombinant protein were pooled, concentrated using an Amicon YM10 membrane (Millipore, Billerica, MA), and fractionated on a HiLoad 26/60 Superdex 75 pg column (Amersham Biosciences) equilibrated in 25 mM Tris (pH 7.2), 600 mM NaCl buffer. Aa-RNase III-containing fractions

(330–560 mM NaCl) were pooled and diluted with a 50 mM Tris (pH 7.5) buffer to reduce the NaCl concentration to 300 mM. The sample was applied to a 15 ml AGPoly(I)•Poly(C) Type 6 column (Amersham Biosciences) equilibrated with 50 mM Tris (pH 7.5), 300 mM NaCl buffer. The column was washed extensively with equilibration buffer until a stable baseline was reached and then eluted with a linear gradient of NaCl from 0.3 to 1 M. Fractions containing recombinant protein were pooled, concentrated, and subjected to a second round of size exclusion chromatography as described above. The final product was diluted with a 25 mM Tris (pH 7.2) buffer to reduce the NaCl concentration to 300 mM and concentrated to 17.4 mg/ml (determined spectrophotometrically using a molar extinction coefficient of 24,180 M^{-1} cm^{-1}). Aliquots were flash-frozen in liquid nitrogen and stored at −80°C until use. The Aa-RNase III protein was judged to be >95% pure by sodium dodecyl sulfate-polyacrylamide gel electrophoresis. The molecular weight was confirmed by electrospray mass spectrometry.

The purification protocol for E110Q was identical to that for E110K. For E110Q, the final concentration was 18.1 mg/ml. The molar extinction coefficient for E110Q was the same as for E110K (24,180 M^{-1} cm^{-1}).

RNAs 2, 3, and 4

RNA 2 (11-mer, 5′-CGAACUUCGCG-3′), RNA 3 (12-mer, 5′-AAAUA UAUAUUU-3′), and RNA 4 (12-mer, 5′-CGCGAAUUCGCG-3′) were purchased from Integrated DNA Technologies (Coralville, IA) and dissolved at 0.75 mM concentration in 25 mM Tris-HCl (pH 7.2) buffer containing 0.1 M NaCl.

Crystallization and X-Ray Diffraction Data Collection

Single crystals were grown using the hanging drop vapor diffusion method at 19 ± 1°C. The drops contained equal volumes of the protein and reservoir solutions. For Aa-E110Q, the protein concentration was 0.0375 mM (10 mg/ml) and RNA concentration was 0.075 mM in 25 mM Tris-HCl (pH 7.2) containing 200 mM NaCl. For Aa-RNase III and Aa-E110K, the concentrations of protein and RNA were the same as for Aa-E110Q, but with the addition of 1.5 mM $CaCl_2$ and 1.5 mM $MgCl_2$, respectively. For Aa-E110Q•2-2, the reservoir solution was composed of 2.0 M ammonium sulfate in 0.1 M HEPES (pH 7.5). For Aa-RNase III•3-3, the reservoir solution was composed of 12%–14% (w/v) PEG 4000, 14%–16% (w/v) isopropanol in 0.1 M trisodium citrate (pH 5.6) buffer. The reservoir solution for both Aa-RNase III•4-4 and Aa-E110K•4-4 was composed of 0.1 M magnesium formate and 14%–16% (w/v) PEG 3350. The X-ray diffraction data were collected at the Southeast Regional Collaborative Access Team (SER-CAT) insertion device beamline 22-ID at the Advanced Photon Source (APS), Argonne National Laboratory. Data processing was carried out with the HKL2000 program suite (Otwinowski and Minor, 1997). Crystal data and processing statistics are summarized in Table 1. Further data processing was carried out with the CCP4 suite (CCP4, 1994) for structure determination.

Structure Solution and Refinement

The structures of Aa-E110Q•2-2, Aa-RNase III•3-3, and Aa-RNase III•4-4 were solved with the molecular replacement program AMoRe (Navaza, 1994); the dimer of ligand-free Aa-endoND structure (Blaszczyk et al., 2001) was the search model after all solvent molecules were removed. The partial structures, each containing two endoNDs, were subjected to rigid body refinement, energy minimization, and grouped B factor refinement followed by a difference Fourier synthesis, which revealed the position of dsRBD and dsRNA. The complete models were built accordingly. The structure of Aa-E110K•4-4 was determined with the difference Fourier method based on the refined structure of Aa-RNase III•4-4 (this work), from which the water molecules were removed before initial Fourier synthesis was carried out.

The refinement of all four structures was done with the program CNS (Brünger et al., 1998) on a Silicon Graphics Fuel workstation (Mountain View, CA). Bulk solvent correction was employed. During the refinement, the $2F_o - F_c$ and $F_o - F_c$ electron density maps were regularly calculated for inspecting and improving the model. Solvent molecules, as peaks $\geq 3\ \sigma$ on the $F_o - F_c$ electron density map with reasonable hydrogen bond network, were included as water molecules in the model at the later stage of the refinement and verified with omit maps. All graphics work was carried out using O (Jones et al., 1991). The refined structures were assessed using PROCHECK (Laskowski et al., 1993). Illustrations were prepared with the program packages MOLSCRIPT (Kraulis, 1991), BOBSCRIPT (Esnouf, 1997), RASTER3D (Merritt and Bacon, 1997), and GRASP (Nicholls et al., 1991).

Acknowledgments

We thank Scott Cherry for help with protein expression, Sergey Tarasov for assistance with mass spectrometry, Zhongmin Jin for assistance during X-ray diffraction data acquisition, and Alexander Wlodawer and Allen Nicholson for critical reading of the manuscript. Electrospray mass spectrometry experiments were conducted on the LC/ESMS instrument maintained by the Biophysics Resource in the Structural Biophysics Laboratory, National Cancer Institute. X-ray diffraction data were collected at the SER-CAT 22-ID beamline at the Advanced Photon Source, Argonne National Laboratory. Supporting institutions may be found at http://www.ser-cat.org/members.html.

Received: May 19, 2005
Revised: June 28, 2005
Accepted: June 29, 2005
Published: October 11, 2005

References

Bardwell, J.C., Regnier, P., Chen, S.M., Nakamura, Y., Grunberg-Manago, M., and Court, D.L. (1989). Autoregulation of RNase III operon by mRNA processing. EMBO J. *8*, 3401–3407.

Bernstein, E., Caudy, A.A., Hammond, S.M., and Hannon, G.J. (2001). Role for a bidentate ribonuclease in the initiation step of RNA interference. Nature *409*, 363–366.

Blaszczyk, J., Tropea, J.E., Bubunenko, M., Routzahn, K.M., Waugh, D.S., Court, D.L., and Ji, X. (2001). Crystallographic and modeling studies of RNase III suggest a mechanism for double-stranded RNA cleavage. Structure *9*, 1225–1236.

Blaszczyk, J., Gan, J., Tropea, J.E., Court, D.L., Waugh, D.S., and Ji, X. (2004). Noncatalytic assembly of ribonuclease III with double-stranded RNA. Structure *12*, 457–466.

Brünger, A.T., Adams, P.D., Clore, G.M., DeLano, W.L., Gros, P., Grosse-Kunstleve, R.W., Jiang, J.S., Kuszewski, J., Nilges, M., Pannu, N.S., et al. (1998). Crystallography & NMR system: a new software suite for macromolecular structure determination. Acta Crystallogr. D Biol. Crystallogr. *54*, 905–921.

Calin-Jageman, I., and Nicholson, A.W. (2003). RNA structure-dependent uncoupling of substrate recognition and cleavage by *Escherichia coli* ribonuclease III. Nucleic Acids Res. *31*, 2381–2392.

Campbell, F.E., Jr., Cassano, A.G., Anderson, V.E., and Harris, M.E. (2002). Pre-steady-state and stopped-flow fluorescence analysis of *Escherichia coli* ribonuclease III: insights into mechanism and conformational changes associated with binding and catalysis. J. Mol. Biol. *317*, 21–40.

Carthew, R.W. (2001). Gene silencing by double-stranded RNA. Curr. Opin. Cell Biol. *13*, 244–248.

CCP4 (Collaborative Computational Project, Number 4)(1994). The CCP4 suite: programs for protein crystallography. Acta Crystallogr. D Biol. Crystallogr. *50*, 760.

Court, D. (1993). RNA processing and degradation by RNase III. In Control of Messenger RNA Stability, J.G. Belasco and G. Braverman, eds. (New York: Academic Press), pp. 71–116.

Dasgupta, S., Fernandez, L., Kameyama, L., Inada, T., Nakamura, Y., Pappas, A., and Court, D.L. (1998). Genetic uncoupling of the dsRNA-binding and RNA cleavage activities of the *Escherichia coli* endoribonuclease RNase III—the effect of dsRNA binding on gene expression. Mol. Microbiol. *28*, 629–640.

Dunn, J.J. (1982). Ribonuclease III. In The Enzymes, P. Boyer, ed. (New York: Academic Press), pp. 485–499.

Esnouf, R.M. (1997). An extensively modified version of MolScript that includes greatly enhanced coloring capabilities. J. Mol. Graph. Model. *15*, 132–134.

Filippov, V., Solovyev, V., Filippova, M., and Gill, S.S. (2000). A novel type of RNase III family proteins in eukaryotes. Gene *245*, 213–221.

Ho, S.N., Hunt, H.D., Horton, R.M., Pullen, J.K., and Pease, L.R. (1989). Site-directed mutagenesis by overlap extension using the polymerase chain reaction. Gene *77*, 51–59.

Inada, T., and Nakamura, Y. (1995). Lethal double-stranded RNA processing activity of ribonuclease III in the absence of suhB protein of *Escherichia coli*. Biochimie *77*, 294–302.

Inada, T., Kawakami, K., Chen, S.M., Takiff, H.E., Court, D.L., and Nakamura, Y. (1989). Temperature-sensitive lethal mutant of ERA, a G protein in *Escherichia coli*. J. Bacteriol. *171*, 5017–5024.

Jones, T.A., Zou, J.Y., Cowan, S.W., and Kjeldgaard, M. (1991). Improved methods for building protein models in electron density maps and the location of errors in these models. Acta Crystallogr. A *47*, 110–119.

Krainer, A. (1997). Eukaryotic mRNA Processing (New York: IRL Press).

Kraulis, P.J. (1991). MOLSCRIPT: a program to produce both detailed and schematic plots of protein structures. J. Appl. Crystallogr. *24*, 946–950.

Krovat, B.C., and Jantsch, M.F. (1996). Comparative mutational analysis of the double-stranded RNA binding domains of *Xenopus laevis* RNA-binding protein A. J. Biol. Chem. *271*, 28112–28119.

Laskowski, R.A., MacArthur, M.W., Moss, D.S., and Thornton, J.M. (1993). PROCHECK: a program to check stereochemical quality of protein structures. J. Appl. Crystallogr. *26*, 283–291.

Li, H., and Nicholson, A.W. (1996). Defining the enzyme binding domain of a ribonuclease III processing signal. Ethylation interference and hydroxyl radical footprinting using catalytically inactive RNase III mutants. EMBO J. *15*, 1421–1433.

Manche, L., Green, S.R., Schmedt, C., and Mathews, M.B. (1992). Interactions between double-stranded RNA regulators and the protein kinase DAI. Mol. Cell. Biol. *12*, 5238–5248.

Merritt, E.A., and Bacon, D.J. (1997). Raster3D: photorealistic molecular graphics. Methods Enzymol. *277*, 505–524.

Miller, J.H. (1972). Experiments in Molecular Genetics (Cold Spring Harbor, NY: Cold Spring Harbor Laboratory).

Navaza, J. (1994). An automated package for molecular replacement. Acta Crystallogr. A *50*, 157–163.

Nicholls, A., Sharp, K.A., and Honig, B. (1991). Protein folding and association: insights from the interfacial and thermodynamic properties of hydrocarbons. Proteins *11*, 281–296.

Nicholson, A.W. (1996). Structure, reactivity, and biology of double-stranded RNA. Prog. Nucleic Acid Res. Mol. Biol. *52*, 1–65.

Nicholson, A.W. (1999). Function, mechanism and regulation of bacterial ribonucleases. FEMS Microbiol. Rev. *23*, 371–390.

Oppenheim, A.B., Kornitzer, D., Altuvia, S., and Court, D.L. (1993). Posttranscriptional control of the lysogenic pathway in bacteriophage λ. Prog. Nucleic Acid Res. Mol. Biol. *46*, 37–49.

Otwinowski, Z., and Minor, W. (1997). Processing of X-ray diffraction data collected in oscillation mode. Methods Enzymol. *276*, 307–326.

Polson, A.G., and Bass, B.L. (1994). Preferential selection of adenosines for modification by double-stranded RNA adenosine deaminase. EMBO J. *13*, 5701–5711.

Robertson, H.D. (1982). *Escherichia coli* ribonuclease III cleavage sites. Cell *30*, 669–672.

Robertson, H.D., and Dunn, J.J. (1975). Ribonucleic acid processing activity of *Escherichia coli* ribonuclease III. J. Biol. Chem. *250*, 3050–3056.

Robertson, H.D., Webster, R.E., and Zinder, N.D. (1968). Purification and properties of ribonuclease III from *Escherichia coli*. J. Biol. Chem. *243*, 82–91.

Ryter, J.M., and Schultz, S.C. (1998). Molecular basis of double-stranded RNA-protein interactions: structure of a dsRNA-binding domain complexed with dsRNA. EMBO J. *17*, 7505–7513.

Sun, W., and Nicholson, A.W. (2001). Mechanism of action of *Escherichia coli* ribonuclease III. Stringent chemical requirement for the glutamic acid 117 side chain and Mn(2+) rescue of the Glu117Asp mutant. Biochemistry *40*, 5102–5110.

Wu, H., Xu, H., Miraglia, L.J., and Crooke, S.T. (2000). Human RNase III is a 160-kDa protein involved in preribosomal RNA processing. J. Biol. Chem. *275*, 36957–36965.

Zhang, H., Kolb, F.A., Jaskiewicz, L., Westhof, E., and Filipowicz, W. (2004). Single processing center models for human Dicer and bacterial RNase III. Cell *118*, 57–68.

Accession Numbers

The coordinates and structure factors of the four crystal structures (codes 1YZ9, 1YYW, 1YYO, and 1YYK for Aa-E110Q•2-2, Aa-RNase III•3-3, Aa-RNase III•4-4, and Aa-E110K•4-4, respectively) have been deposited with the Protein Data Bank (Rutgers State University of New Jersey).